Biophysical Chemistry 253 (2019) 106231

Contents lists available at ScienceDirect

Biophysical Chemistry

journal homepage: www.elsevier.com/locate/biophyschem

Amyloid jams: Mechanical and dynamical properties of an amyloid fibrillar network

Vincenzo Martorana, Samuele Raccosta, Daniela Giacomazza, Lorena Anna Ditta, Rosina Noto, Pier Luigi San Biagio, Mauro Manno*

National Research Council of Italy, Institute of Biophysics, via Ugo La Malfa 153, 90146 Palermo, Italy

GRAPHICAL ABSTRACT

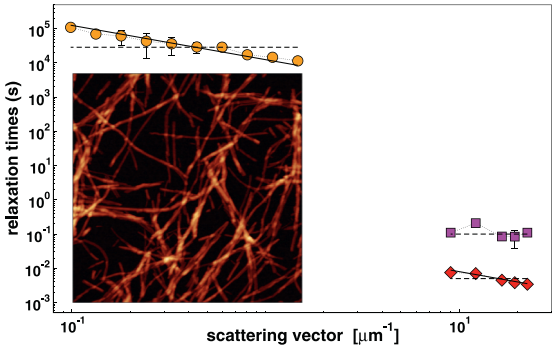

ARTICLE INFO

Keywords:
Amyloid fibrils
Gels
Insulin
Non-ergodicity
Dynamic light scattering

ABSTRACT

Amyloid fibrils have well known pathological implications as well as a clear functional role in different biological systems due to their peculiar structural and mechanical properties. We had previously shown the appearance of elastic properties during the formation of a gel of insulin amyloid fibrils. Here, we study the morphological, rheological and dynamical behaviour of this jammed system. We observe different non-diffusive relaxation processes over a wide length and time interval, suggesting the formation of an elastic transient network of fibrils, and evidencing the structural heterogeneity of the gel matrix and the peculiarity of this potentially new material.

1. Introduction

Amyloid fibrils are ordered elongated protein aggregates, exhibiting a peculiar cross-β sheet quaternary structure along the main fiber axis [1]. Amyloid deposits are associated with protein misfolding diseases, including several neurodegenerative diseases [2]. In addition to their clinical relevance, amyloids have a less known important functional role in different biological environments, where they operate a positive physiological activity [3]. Some bacteria, for instance, use extracellular amyloid matrices to improve surface adhesion and colony proliferation [4]. In general, functional amyloids have been identified in lower organisms, such as bacteria, fungi or insects, as well as in mammalian cells [3]. Indeed, amyloids may be used as important structural components, since they have peculiar mechanical and biological properties [5], such as a high yield-strength and high protease or thermal resistance, that make them resembling the natural silk fibers or other

* Corresponding author.
E-mail address: mauro.manno@cnr.it (M. Manno).

https://doi.org/10.1016/j.bpc.2019.106231
Received 29 June 2019; Accepted 21 July 2019
Available online 24 July 2019

synthetic cross-linked materials [6,7]. These properties have stimulated their exploitation as bio-inspired materials [8], e.g. as conductive nanowires [9], fibers able to capture carbon dioxide [10], or amyloid-graphene nanocomposites [11].

In our previous work, we have shown the appearance of a significant elastic network of insulin amyloid fibers, associated to fibril elongation more than to the formation of large structures and the eventual amyloid gel [12]. Insulin has long been known to form amyloid fibrils under acidic conditions [13], and it has been studied extensively as a model system for amyloid fibrillation [14–17]. Insulin aggregation is enriched by a complex hierarchy of different morphologies, including fibrils, larger bundles and floccules, which may eventually assemble to form a gel [15,18,19]. In the present work, we continue the study of the morphological and mechanical properties of this insulin amyloid gel, with a focus on the dynamical relaxation processes of the amyloid network. In order to address this problem, we exploit the capability of dynamic light scattering techniques at both small and large angle, opportunely adapted to deal with the intrinsic non-ergodicity of gel systems.

We observed different non-diffusive relaxation processes spread over a wide range of time and length scales. While a detailed description of the system dynamics is beyond the scope of this work, we may argue that the slow dynamical relaxation resembles the behaviour of elastic networks with transient topological rearrangements [20]. Along with our rheological and morphological measurements, these dynamical observations strengthen the picture of amyloids as new, strong and malleable materials, which are capable of sustaining stress, as entangled polymers [21] or natural and synthetic fibers [5], and also of retaining self-healing adaptive properties, as flexible transient networks [22].

2. Materials and methods

2.1. Sample preparation

Bovine insulin powder (purchased from SIGMA) was dissolved in 20% w/w acetic acid (reagent grade) and Millipore Super-Q water and filtered through 0.2 μm GV Millex filters. Insulin concentration was measured by UV absorption at 276 nm, with an extinction coefficient of 1.0 $cm^2\,mg^{-1}$ [12]. Insulin solution was incubated at 70 °C for 24 or 48 h either in quartz cells, for scattering measurements, or in glass tubes for other experiments.

2.2. Optical microscopy

The samples were gently removed from the tube and put on glass slides. Optical microscopy images were taken by using an inverted microscope with colour-corrected infinity optical system (MOTIC AE21) and a 1.3 M pixel digital camera [23].

2.3. Atomic force microscopy

30 μL of the incubated samples were gently removed from the glass tube, then either directly used or mixed with 270 μL of buffer. The samples were deposited on a freshly cleaved mica substrate, incubated at room temperature for 15 min and gently washed with buffer. Atomic force microscopy images were taken by a JPK Nanowizard 3, operating in air tapping mode with a rate of 1 Hz (resolution 512 × 512), a set point fixed at 20 nm (80% of the free amplitude), and using NSC15 MikroMasch cantilevers (resonance frequency 290 kHz, nominal spring constant 40 $N \cdot m^{-1}$), equipped with silicon tips with a typical radius of curvature of 8 nm.

2.4. Rheological measurements

Incubated samples were gently removed from the tube and put on the plate of a stress-controlled rheometer with a temperature control within 0.1 °C (AR1000, TA Instruments UK). Viscoelastic spectra and shear rate ramps were measured at room temperature with a plate-cone geometry, by using an acrylic cone and an angle of less than 1° and a 26 μm truncation gap (T.A. Instruments). The excess sample was blotted away by a filter paper, and paraffin oil (GPR grade, BDH, UK) was layered around exposed sample surfaces. A solvent-trap cover-slip was also used to prevent evaporation. The viscoelastic spectra were taken with a low strain of 0.01, in order to limit sample perturbation.

2.5. Small angle dynamic light scattering (S-DLS)

Small angle light scattering (SALS) experiments were performed by using a home-made light-scattering apparatus [15,23,24] equipped with a charge-coupled device Pulnix TM765 camera and a He−Ne laser operating at a wavelength of 632.8 nm. The instrument operates over a range of scattering angle from 0.1° to 11°, corresponding to scattering vector magnitudes between 0.02 and 2 μm^{-1}. After 48-hour incubation into quartz cells with an optical path of 2 mm, the measurements were taken at room temperature for one day. The average scattered intensity was checked to be stationary for the course of the measurement. The intensity auto-correlation functions $g_2(t)$ were computed by using a home made software code. The electric field correlation functions $g_E(t)$ were recovered from the single pixel intensity correlation functions, correcting for the presence of a static stray light contribution. The ensemble average of the correlation functions, necessary in the case of non ergodic systems, is allowed by the multi-pixel CCD sensor [25].

2.6. Large angle dynamic light scattering (L-DLS)

Samples were incubated into quartz cells and then placed at room temperature in a Brookhaven Instrument BI200-SM Goniometer, equipped with an Argon laser tuned at 514.5 nm. The intensity auto-correlation functions $g_2(t)$ were measured at different scattering vectors by a Brookhaven Instrument BI-9000 correlator.

3. Results and discussion

Insulin fibrillar samples were prepared by incubating highly concentrated solutions (0.75 and 2.0 mM), at high temperature (70 °C). Insulin powder was dissolved in 20% Acetic Acid aqueous solution, pH 1.9. In such conditions, insulin is known to be monomeric and to form amyloid fibril upon incubation at high temperature [12,26]. After one or two days of incubation at 70 °C, insulin samples become highly viscous due to the formation of large size aggregates. Indeed, insulin fibrillation initiates by the elongation of single amyloid fibers and then proceeds by a cascade of different processes, including secondary nucleation, branching and fiber assembly, thus resulting in the formation of a complex hierarchy of different structures [15,17]. As expected from previous work [16,18,27], we observed the presence of bundles of amyloid fibers (Fig. 1a), a network of entangled elongated amyloid fibrils (Fig. 1c,d), and single (moderately branched) fibrils (Fig. 1e,f), with an apparent width of about 25 nm, and a length up to a few microns. We also detected the sporadic presence of amyloid spherulites (Fig. 1b), aggregates with a radial orientation of fibrils, which have been observed in different conditions [17,27].

In a previous work [12], we observed the formation of an elastic network of insulin fibrils upon heating on the same experimental conditions used in the present work. A significant growth of the elastic modulus was detected during fiber elongation. Now we investigate the mechanical properties of the same samples after one or two days of heating. The macroscopic aspect of these samples is that of a viscous slurry, or eventually a soft gel. Indeed, the viscoelastic spectra exhibit a flat frequency dependence of the viscoelastic moduli over more than two decades (Fig. 2a). The elastic part of the modulus G' is significantly higher than the dissipative one G'', thus indicating a clear gel-like

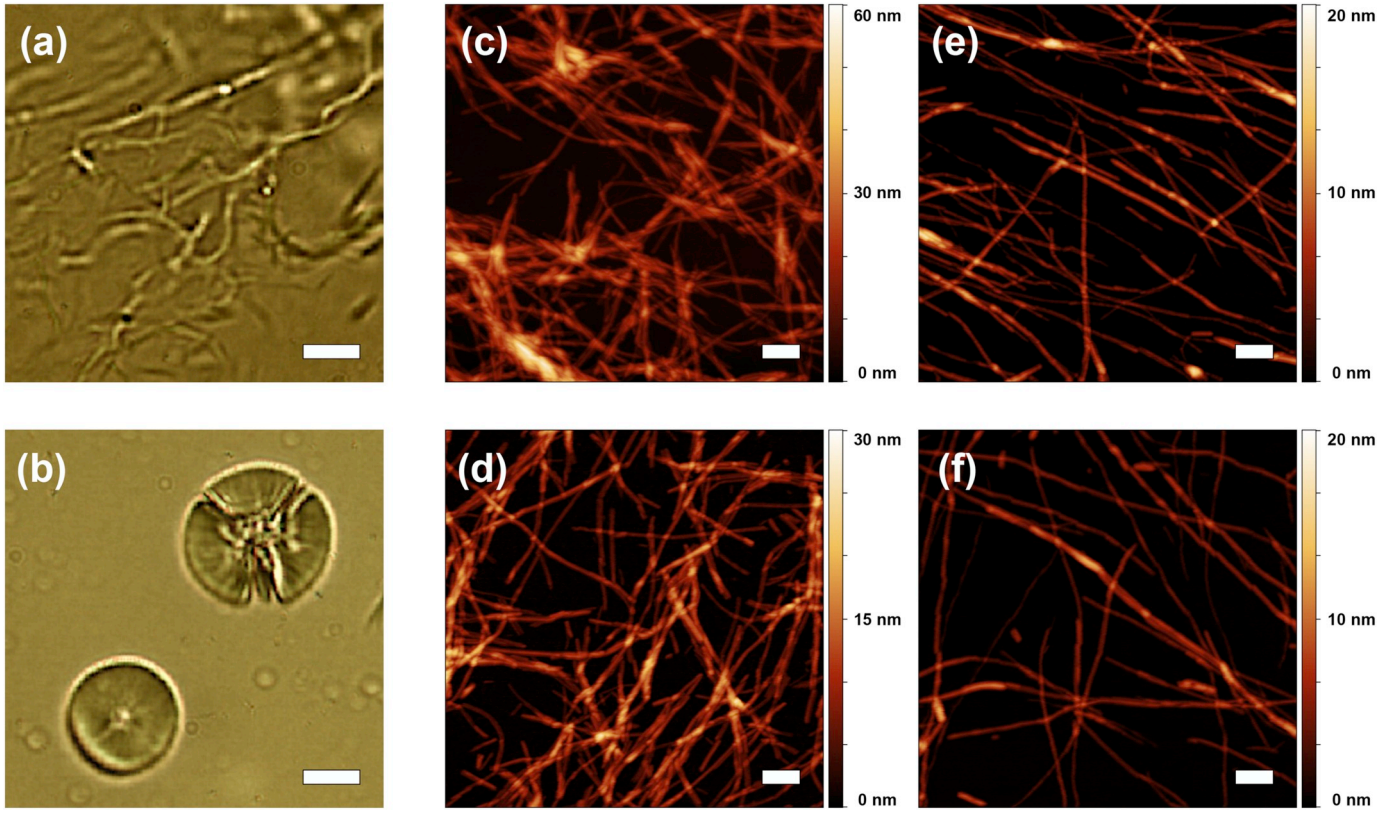

Fig. 1. Optical microscopy (a,b) and atomic force microscopy (c,d,e,f) images of insulin solutions after 24 h of incubation at 70 °C. Optical microscopy: (a,b) 2 mM; the horizontal bars are 10 μm; atomic force microscopy: (c) 2 mM; (d) 2 mM diluted 1:10; (e) 0.75 mM; (f) 0.75 mM diluted 1:10; the horizontal bars are 200 nm;

behaviour [28]. Also, the measurements of dynamic viscosity η at increasing shear rate $\dot{\gamma}$, show another characteristics of elastic networks, that is the shear thinning behaviour (Fig. 2b). The $\eta(\dot{\gamma})$ curves can be represented by the classical empirical Sisko model, using the expression [29]:

$$\eta = \eta_{\infty} + m\dot{\gamma}^{n-1} \tag{1}$$

where $n = 0.2$ is the exponent describing the departure from Newtonian behaviour ($n = 1$), and η_{∞} is the viscosity at infinite shear rate, when entangled structures or large clusters are disassembled. At both concentrations we found the same value $\eta_{\infty} = 4.5 \cdot 10^{-3} Pa \cdot s$, slightly higher then solvent viscosity, as typically observed in other colloidal or protein aggregate systems [23,30].

The dynamical behaviour of insulin jammed samples was studied on different spatial and time scales by using both small angle and large multi-angle dynamic light scattering. Such experiments require a particular care, since the system under study exhibits a non-ergodic behaviour [31], on microscopic and mesoscopic time-scales, from microseconds to seconds, mirroring the gel-like mechanical and structural properties of these jammed entangled networks (Figs. 1, 2). This operatively means that the ensemble-averaged values of physical quantities cannot be obtained from ordinary time-averages, and that different volumes of the sample yield different values of the measured quantities. We detected non-ergodic behaviour in large angle light scattering experiments by moving vertically the couvette and measuring scattering intensity. The average intensity values were different at different positions of the cell (data not shown). In such cases, ergodicity may be restored by performing spatial averaging over different parts of the sample [32]. Such a procedure may be performed e.g. by automatically moving the sample in large angle light scattering measurements [32,33], while it is automatically achieved in small angle dynamic light scattering experiments, since for each scattering vector the intensity is averaged over many pixels of the detecting CCD camera [15,25].

Small angle dynamic light scattering (S-DLS) experiments were performed on samples incubated at high temperatures for 2 days. The intensity auto-correlation function $g_2(t)$ was computed by using a home made software, then the electric field correlation function $g_E(t)$ was obtained by using the procedure described in Cipelletti and Weitz 1999 [25]. Fig. 3 shows the correlation functions $g_E(t)$ at different scattering vectors, corresponding to dynamical relaxations occurring on length-scales from a few micrometers to tens of micrometers. The correlation functions exhibit a clear non exponential behaviour and can be fitted by the expression:

$$g_E(t) = c_0 + \exp\{-(t/\tau_0)^{\gamma_0}\} \tag{2}$$

which contains a constant c_0 and a compressed exponential with exponent γ_0 in the range $1.7 - 1.9$. The characteristic times at different scattering vectors have an average value of 8 h, and display a slight q-dependence, definitively related neither to a diffusive relaxation process ($\tau \sim q^{-2}$) [34], nor to the dynamical relaxation of an entangled polymer network ($\tau \sim q^{-3}$ or $\tau \sim q^{-4}$) [35]. In the inset of Fig. 3, an inverse q dependence is drawn with the expression: $\tau_0 = (v_0 q)^{-1}$, with $v_0 = 8 \cdot 10^{-5}\ \mu m \cdot s^{-1}$.

Further, large angle dynamic light scattering (L-DLS) experiments were performed on samples incubated at high temperatures for 2 days. Fig. 4 shows the normalised intensity auto-correlation functions at different scattering vectors (as displayed in the legend), which in this case correspond to the dynamical relaxations occurring on length-scale of hundreds of nanometers.

At large angles, time-averaging is again not sufficient to restore ergodicity, and spatial averaging should be performed by moving the sample or the detector. Alternatively, the intensity auto-correlation functions $g_2(t)$ may be obtained by a "heterodyne" approach [31]. The

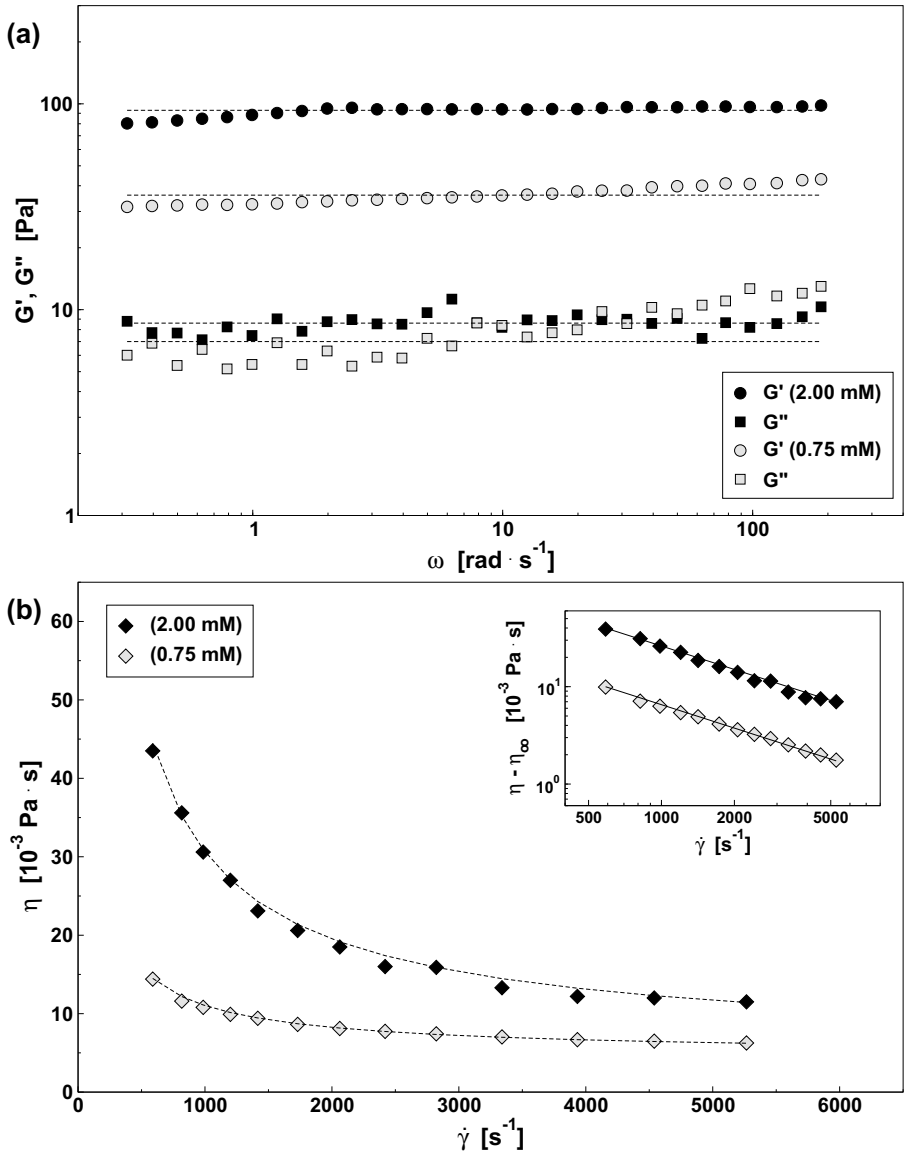

Fig. 2. Rheological characterisation of 2.0 and 0.75 mM insulin samples after 24 h of incubation at 70 °C. (a) Viscoelastic spectra: elastic (G') and dissipative (G'') parts, the dashed lines are the average values over the frequency range; (b) viscosity η vs shear rate $\dot{\gamma}$, the dashed lines are the best fit by the Sisko model; the inset reports the same curves in a log-log plot after subtraction of infinite shear rate viscosity η_∞.

scattered electric field is partitioned into a slow contribution $E_S(t)$, which does not decay during the time of the measurement, and a fast fluctuating contribution $E_F(t)$, related to dynamical relaxation within the gel matrix. The correlation function of the fast field $g_F(t)$ is derived by beating with the slow component and it is related to the intensity correlation function $g_2(t)$, by the relation:

$$\frac{g_2(t)-1}{g_2(0)-1} = a\,|g_F(t)|^2 + [1-a]g_F(t) \tag{3}$$

with $a^{-1} = 1 + 2\rho i_S/i_F$, where i_F and i_S are the average intensities of the fast and slow components respectively, and the optical mixing coefficient $\rho = \alpha^2\beta^{-1}$ is the ratio of two factors dependent on the optical geometry and related to the complex coherent factor [25,36].

The correlation functions clearly reveal different non exponential relaxations, which can be fitted by using two stretched exponential functions [37,38]:

$$g_F(t) = a_0 + a_1\exp\{-[t/\tau_1]^{\gamma_1}\} + a_2\exp\{-[t/\tau_2]^{\gamma_2}\} \tag{4}$$

with the exponents γ_1 and γ_2 included in the range $0.35 - 0.42$ and $0.6 - 0.7$, respectively. The larger characteristic time τ_1 has an average value of 100 ms and shows no q-dependence. The shorter characteristic time τ_2 has an average value of 5 ms and shows a poor q-dependence. Also in this case, the process is clearly neither diffusive, nor related to polymer network collective relaxation. In the inset of Fig. 4, an inverse q dependence is drawn with the expression: $\tau_2 = (\nu_2 q)^{-1}$, with $\nu_2 = 8\cdot 10^{-2}\,\mu m\cdot s^{-1}$.

The fast fluctuating fraction x_F ($x_F = i_F/[i_F + i_S]$) can be determined for each measurement of Fig. 4 by analysing the intensity time series collected during the experiment. The insets of Fig. 5 report the intensity $I_{\delta t}$ integrated over an interval $\delta t \le 1s$, normalised with respect to the average value $\langle I_{\delta t}\rangle$. The corresponding distribution functions $P(I_{\delta t})$ are reported in Fig. 5. The scattered electric field can be partitioned in a fast component E_F and a slow component E_S, which is static with respect to the interval $\delta t \approx 1s$. Since the correlation function are also measured up to a time delay of a few seconds (Fig. 4), we may consider that the fast contribution related to $I_{\delta t}$ matches the fast fluctuating contribution of the heterodyne correlation functions. By extending a previous theory [39,40], we had shown that the normalised intensity distribution

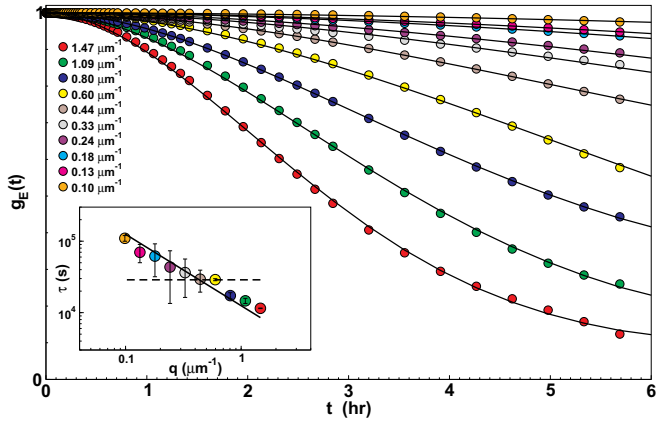

Fig. 3. Small angle dynamic light scattering correlation functions of 2 mM insulin gels incubated for 2 days at 70 °C, at different scattering angles as in the legend. Solid curves are best fit to data. Inset: characteristic times τ_0 (circles) obtained from fitting; the dashed line marks the average value, the solid lines indicates a q^{-1} behaviour.

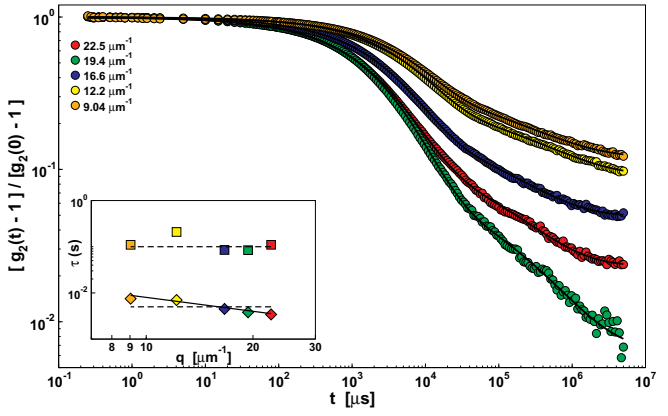

Fig. 4. Large angle dynamic light scattering correlation functions of 0.75 mM insulin gels incubated for 2 days at 70 °C, at different scattering angles as in the legend. Solid curves are best fit to data. Inset: characteristic times τ_1 (squares) and τ_2 (diamonds) obtained from fitting; the dashed lines mark the average values, the solid line indicates a q^{-1} behaviour.

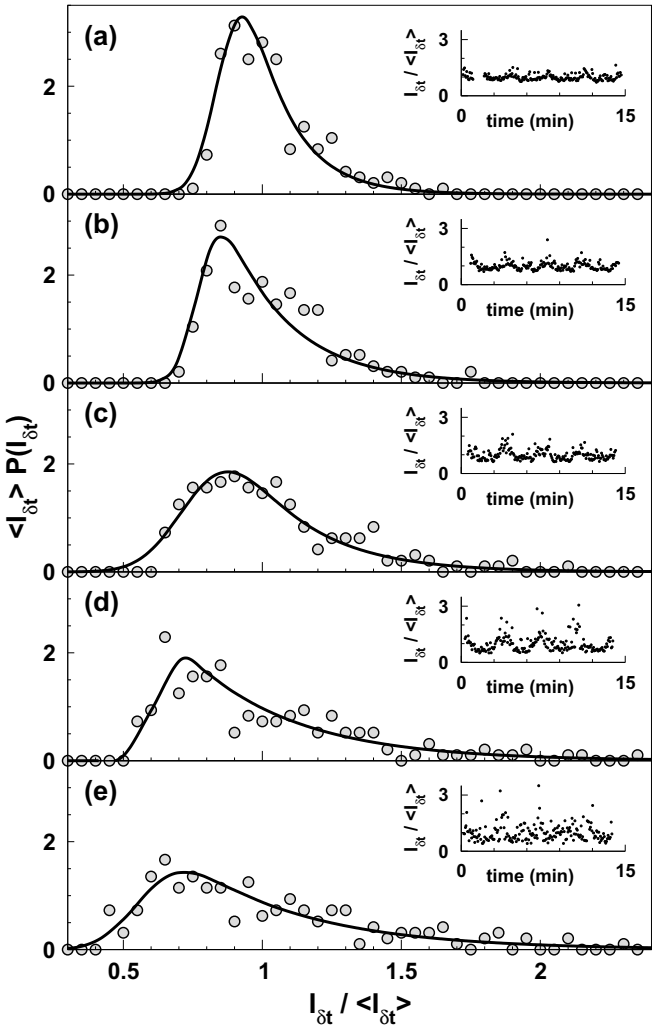

Fig. 5. Intensity distribution functions a 0.75 mM insulin sample after 48 h of incubation at 70 °C, at different scattering angles: 90° (a), 75° (b), 63° (c), 45° (d) and 33° (e). The insets show the corresponding intensity $I_{\delta t}$ time series normalised with the average value $\langle I_{\delta t} \rangle$.

functions can be fitted with the convolution of two terms [19,32,33]: a Gaussian distribution related to the fast component with average x_F and variance ${x_F}^2/N$, where N is a number reminiscent of the ratio between the integration interval δt and the coherence time of the field, and an exponential distribution related to the slow field, with average $1 - i_F$. The x_F values obtained by the intensity distribution (Fig. 5) match the values obtained by the parameters a used in the heterodyne computation of the correlation function (Fig. 5 and Eq. (4)), with the reasonable assumption $\rho \sim 1$.

4. Conclusions

In the present work, we have studied the mechanical, dynamical and structural properties of a network made of amyloid insulin fibrils, and exhibiting a gel-like behaviour. In a previous work, we have shown that a significant elastic shear modulus is produced by the initial formation of elongated aggregates occurring during the "apparent" lag-phase [12]. Here, we confirm that the formation of large fibrillar aggregates builds an entangled amyloid network and determines a macroscopic or mesoscopic gel-like behaviour (Figs. 1 and 2). By using the appropriate theoretical and experimental tools developed to deal with non-ergodic systems [19,25,31–33], the dynamical relaxation modes have been monitored by large and small angle dynamic light scattering. We found the existence of different non-diffusive relaxation processes on wide range of spatial and time scales (Figs. 3 and 4). The larger process on the micrometer length scale has characteristic times of the order of a few hours and a probable q^{-1} dependence. This behaviour is reminiscent of a phonon-assisted relaxation, that is a process exhibiting a linear dependence of the relaxation rate upon the scattering vector. By assuming that such a relaxation is due to phonon propagation with a velocity $v_0 = 8 \cdot 10^{-5}\, \mu m \cdot s^{-1}$, one could estimate the resulting elastic modulus G by the classical expression $G \approx \rho {v_0}^2$, where ρ is the density, taken as $1\ g \cdot cm^3$. Therefore, one obtains a value of G of the order of a few pico Pascal, which is far below the values obtained from rheological experiments. At smaller length scales, we also observe two non-diffusional relaxation processes, with almost no q-dependence.

The origin of this relaxation is not clear. A similar dependence of characteristic time has been attributed to local shrinking of gel structure, causing local inhomogenieties [41], or to the influence on bulk elasticity of loop defects in polymer networks [42]. A flat or quasi-flat q-dependence of relaxation times has also been observed in PVA and PS polymers [37,43,44] and, more recently, in DNA nanostars [38,45], used to mimic low-valence colloids [46]. The proposed explanation assigns the slow relaxation modes to topological rearrangements in the network, which determine fluctuations in the local bulk modulus, thus

allowing concentration fluctuations in absence of mass transport. While a clear explanation is still missing, in the present work we report these peculiar relaxation modes, likely related to local network rearrangements, for the case of an amyloid jammed system, that is a transient network of irreversible amyloid aggregates. We believe these findings may open new perspectives and stimulate further studies of this "amyloid jam", that is a fragile matrix made of strong amyloid units.

Acknowledgement

We are grateful to D. Bulone, A. Emanuele and J. Newman for the countless discussions made over many years on this subject. We acknowledge the professional support of F. Giambertone and M. Lapis for the development of software and scattering devices, and of F. D'Anca and R. Megna for the design and fabrication of different mechanical components.

Appendix A. DLS with a slow contribution: ensemble averaging and heterodyne approach

In the classical approach for scattering by non-ergodic samples [31], the scattered electric field $E(t)$ is considered as the sum of a fast contribution $E_F(t)$, and a slow contribution $E_S(t)$. The scattered intensity $I(t) = E(t)E^*(t)$ can be written as:

$$I(t) = [E_F(t) + E_S(t)][E_F^*(t) + E_S^*(t)] + I_D(t) \tag{A.1}$$

where we added a term related to the dark current I_D. The intensity correlation $G(t) = \langle I(0)I(t)\rangle$ can be expressed in terms of the different components:

$$G(t) = G_D(t) + G_F(t) + G_S(t) + 2G_{FS}(t) + 2i_F i_S + 2i_D i_F + 2i_D i_S \tag{A.2}$$

The quantities used in the latter expression are defined below in Table A.1.

Table A.1
Different radiation components and related quantities. The brackets < > indicates a time averaging.

"Fast" field $E_F(t)$	$i_F = \langle E_F E_F^* \rangle$
$I_F(t) = E_F(t)E_F^*(t)$	$\sigma_F^2 = i_F^{-1}[\langle I_F^2\rangle - i_F^2]$
	$G_F(t) = \langle I_F(0)I_F(t)\rangle$
	$g_F(t) = i_F^{-1}\langle E_F(0)E_F^*(t)\rangle$
"Slow" field $E_S(t)$	$i_S = \langle E_S E_S^* \rangle$
$I_S(t) = E_S(t)E_S^*(t)$	$\sigma_S^2 = i_S^{-1}[\langle I_S^2\rangle - i_S^2]$
	$G_S(t) = \langle I_S(0)I_S(t)\rangle$
"Dark" term	$i_D = \langle I_D\rangle$
$I_D(t)$	$\sigma_D^2 = i_D^{-1}[\langle I_D^2\rangle - i_D^2]$
	$G_D(t) = \langle I_D(0)I_D(t)\rangle$
"Mixed" term $E_F(t)E_S^*(t)$	$i_{FS} = \langle I_{FS}\rangle$
$I_{FS}(t) = E_F(t)E_S^*(t)$	$\alpha^2 = (i_F i_S)^{-1}[\langle I_{FS}^2\rangle - i_{FS}^2]$
	$G_{FS}(t) = \langle I_{FS}(0)I_{FS}(t)\rangle$

By taking for each component the properties described below in Table A2, the normalised intensity auto-correlation function $g_2(t) = i^{-1}G(t)$ (where $i = \langle I\rangle$) can be written:

$$g_2(t) - 1 = \beta x_F^2 g_F(t)^2 + \beta x_S^2 \sigma_S^2 + 2\alpha^2 x_F x_S g_F(t) + x_D \sigma_D^2 \delta(t) \tag{A.3}$$

where $x_F = i_F/i$, $x_S = i_S/i$, $x_D = i_D/i$ are the fraction of the fast, slow and dark term, respectively.

This expression can be further simplified if one defines the following quantities (for $t \neq 0$):

$$X = \frac{x_F}{1 - x_D} \tag{A.4}$$

$$h(t) = \frac{g_2(t) - 1}{g_2(0) - 1} \tag{A.5}$$

Table A2
Properties of the different radiation components.

E_F is a Gaussian complex process:
$i_F^{-2}G_F(t) = 1 + \beta\lvert g_F(t)\rvert^2$
E_S has a fixed value:
$i_S^{-2}G_S(t) = 1 + \beta\sigma_S^2$
I_D is dark noise:
$i_D^{-2}G_D(t) = 1 + \sigma_D^2\delta(t)$
E_F E_S are independent fields:
$i_{FS} = 0$, $G_{FS}(t) = \alpha^2 i_F i_S g_F(t)$

One obtains the following expressions:

$$h(t) = h(\infty) + [1 - h(\infty)]f\{ag_F(t)^2 + [1 - a]g_F(t)\} \tag{A.6}$$

$$h(\infty) = \frac{\beta(1-X)^2\sigma_S^2}{\beta X^2 + 2\alpha^2 X(1-X) + \beta(1-X)^2\sigma_S^2} \tag{A.7}$$

$$\frac{1}{a} = 1 + \frac{2\alpha^2}{\beta}\frac{1-X}{X} \tag{A.8}$$

The latter expressions hold for both the ensemble (e.g. spatial) averaging and the heterodyne approach. In the first case, the slow contribution is due to a non relaxing field: ${\sigma_S}^2 = 1$ and $h(\infty) \neq 0$. In the hetorodyne approach, the slow contribution is due to a contribution which is static during the measurement, yet completely uncorrelated: ${\sigma_S}^2 = 0$ and $h(\infty) = 0$. Therefore, the same expression can be used to compute the correlation function in camera-based small angle dynamic light scattering measurements ($g_E(t) = g_F(t)$), with respect to the static stray light [25], and at the same time to fit the fast field in large angle dynamic light scattering measurements, with respect to a slow non-ergodic contribution [31].

References

[1] F. Chiti, C.M. Dobson, Protein misfolding, functional amyloid, and human disease, Annu. Rev. Biochem. 75 (2006) 333–366.
[2] T.P. Knowles, M. Vendruscolo, C.M. Dobson, The amyloid state and its association with protein misfolding diseases, Nat. Rev. Mol. Cell Biol. 15 (2014) 384–396.
[3] D.M. Fowler, A.V. Koulov, W.E. Balch, J.W. Kelly, Functional amyloid - from bacteria to humans, Trends Biochem. Sci. 32 (2007) 217–224.
[4] M.R. Chapman, L.S. Robinson, J.S. Pinkner, R. Roth, J. Heuser, M. Hammar, S. Normark, S.J. Hultgren, Amyloid fiber formation role of *Escherichia coli* curli operons in directing amyloid fiber formation, Science 295 (2002) 851–856.
[5] T.P. Knowles, M.J. Buehler, Nanomechanics of functional and pathological amyloid materials, Nat. Nanotechnol. 6 (2011) 469–479.
[6] U. Slotta, S. Hess, K. Spieß, T. Stromer, L. Serpell, T. Scheibel, Spider silk and amyloid fibrils: a structural comparison, Macromol. Biosci. 7 (2007) 183–188.
[7] I. Cherny, E. Gazit, Amyloids: not only pathological agents but also ordered nanomaterials, Angew. Chem. Int. Ed. 47 (2008) 4062–4069.
[8] T.P. Knowles, R. Mezzenga, Amyloid fibrils as building blocks for natural and artificial functional materials, Adv. Mater. 28 (2016) 6546–6561.
[9] T. Scheibel, R. Parthasarathy, G. Sawicki, X.-M. Lin, H. Jaeger, S.L. Lindquist, Conducting nanowires built by controlled self-assembly of amyloid fibers and selective metal deposition, Proc. Natl. Acad. Sci. U. S. A. 100 (2003) 4527–4532.
[10] D. Li, H. Furukawa, H. Deng, C. Liu, O.M. Yaghi, D.S. Eisenberg, Designed amyloid fibers as materials for selective carbon dioxide capture, Proc. Natl. Acad. Sci. 111 (2014) 191–196.
[11] P. Li, S. Banjade, H.C. Cheng, S. Kim, B. Chen, L. Guo, M. Llaguno, J.V. Hollingsworth, D.S. King, S.F. Banani, P.S. Russo, Q.X. Jiang, B.T. Nixon, M.K. Rosen, Phase transitions in the assembly of multivalent signalling proteins, Nature 483 (2012) 336–340.
[12] M. Manno, D. Giacomazza, J. Newman, V. Martorana, P.L.S. Biagio, Amyloid gels: precocious appearance of elastic properties during the formation of an insulin fibrillar network, Langmuir 26 (2010) 1424–1426.
[13] D.F. Waugh, A mechanism for the formation of fibrils from protein molecules, J. Cell. Physiol. 49 (1957) 145–164.
[14] J.L. Jime'nez, E.J. Nettleton, M. Bouchard, C.V. Robinson, C.M. Dobson, H.R. Saibil, The protofilament structure of insulin amyloid fibrils, Proceedings of the National Academy of Sciences of the United States of America, 99 2002, pp. 9196–9201.
[15] M. Manno, E.F. Craparo, A. Podesta, D. Bulone, R. Carrotta, V. Martorana, G. Tiana, P.L.S. Biagio, Kinetics of different processes in human insulin amyloid formation, J. Mol. Biol. 366 (2007) 258–274.
[16] R. Jansen, W. Dzwolak, R. RolandWinter, Amyloidogenic self-assembly of insulin aggregates probed by high resolution atomic force microscopy, Biophys. J. 88 (2005) 1344–1353.
[17] V. Vetri, F. Piccirilli, J. Krausser, G. Buscarino, U. Łapińska, B. Vestergaard, A. Zaccone, V. Foderà, Ethanol controls the self-assembly and mesoscopic properties of human insulin amyloid spherulites, J. Phys. Chem. B 122 (2018) 3101–3112.
[18] A. Podestà, G. Tiana, P. Milani, M. Manno, Early events in insulin fibrillization studied by time-lapse atomic force microscopy, Biophys. J. 90 (2006) 589–597.
[19] M. Manno, E.F. Craparo, V. Martorana, D. Bulone, P.L. San Biagio, Kinetics of insulin aggregation: disentanglement of amyloid fibrillation from large-size cluster formation, Biophys. J. 90 (2006) 4585–4591.
[20] G. Nava, M. Rossi, S. Biffi, F. Sciortino, T. Bellini, Fluctuating elasticity mode in transient molecular networks, Phys. Rev. Lett. 119 (2017) 1–5.
[21] P.G. De Gennes, Dynamics of entangled polymer solutions. I. the rouse model, Macromolecules 9 (1976) 587–593.
[22] D. Montarnal, M. Capelot, F. Tournilhac, L. Leibler, Silica-like malleable materials from permanent organic networks, Science 334 (2011) 965–968.
[23] S. Raccosta, M. Manno, D. Bulone, D. Giacomazza, V. Militello, V. Martorana, P.L.S. Biagio, Irreversible gelation of thermally unfolded proteins: structural and mechanical properties of lysozyme aggregates, Eur. Biophys. J. 39 (2010) 1007–1017.
[24] R. Carrotta, J. Barthe's, A. Longo, V. Martorana, M. Manno, G. Portale, P.L.S. Biagio, Large size fibrillar bundles of the Alzheimer amyloid β-protein, Eur. Biophys. J. 36 (2007) 701–709.
[25] L. Cipelletti, D.A. Weitz, Ultralow-angle dynamic light scattering with a charge coupled device camera based multispeckle, multitau correlator, Rev. Sci. Instrum. 70 (1999) 3214–3221.
[26] S. Grudzielanek, R. Jansen, R. Winter, Solvational tuning of the unfolding, aggregation and amyloidogenesis of insulin, J. Mol. Biol. 351 (2005) 879–894.
[27] M.R.H. Krebs, C.E. Macphee, A.F. Miller, I.E. Dunlop, C.M. Dobson, A.M. Donald, The formation of spherulites by amyloid fibrils of bovine insulin, Proc. Natl. Acad. Sci. U. S. A. 101 (2004) 14420–14424.
[28] M. Schleeger, C.C. Vandenakker, T. Deckert-Gaudig, V. Deckert, K.P. Velikov, G. Koenderink, M. Bonn, Amyloids: from molecular structure to mechanical properties, Polymer 54 (2013) 2473–2488.
[29] H.A. Barnes, J.F. Hutton, K. Walters, An Introduction to Rheology, Elsevier, 1989.
[30] C.J. Rueb, C.F. Zukoski, Rheology of suspensions of weakly attractive particles: approach to gelation, J. Rheol. 42 (1998) 1451–1476.
[31] P.N. Pusey, W. Van Megen, Dynamic light scattering by non-ergodic media, Physica A 157 (1989) 705–741.
[32] M. Manno, D. Bulone, V. Martorana, P.L. San Biagio, Ergodic to nonergodic transition monitored by scattered light intensity statistics, Physica A 341 (2004) 40–54.
[33] J. Barthès, D. Bulone, M. Manno, V. Martorana, P.L. San Biagio, A statistical light scattering approach to separating fast and slow dynamics: application to a model system, Eur. Biophys. J. 36 (2007) 743–752.
[34] B.J. Berne, R. Pecora, Dynamic Light Scattering with Applications to Chemistry, Biology, and Physics, John Wiley & Sons, Inc, New York, London, Sidney, Toronto, 1990.
[35] M. Doi, S.F. Edwards, The Theory of Polymer Dynamics, Oxford University Press, 1986.
[36] J.W. Goodman, Statistical Optics, John Wiley & Sons, Inc, New York, 2000.
[37] J. Li, T. Ngai, C. Wu, The slow relaxation mode: from solutions to gel networks, Polym. J. 42 (2010) 609–625.
[38] S. Biffi, R. Cerbino, G. Nava, F. Bomboi, F. Sciortino, T. Bellini, Equilibrium gels of low-valence DNA nanostars: a colloidal model for strong glass formers, Soft Matter 11 (2015) 3132–3138.
[39] J.G.H. Joosten, E.T.F. Gelade, P.N. Pusey, Dynamic light scattering by non-ergodic media: Brownian particles trapped in polyacrylamide gels, Phys. Rev. A 42 (1990) 2161–2175.
[40] J.G.H. Joosten, J.L. McCarthy, P.N. Pusey, Dynamic and static light scattering by aqueous polyacrylamide gels, Macromolecules 24 (1991) 6690–6699.
[41] L. Cipelletti, S. Manley, R.C. Ball, D.A. Weitz, Universal aging features in the restructuring of fractal colloidal, Phys. Rev. Lett. 84 (2000) 2275–2278.
[42] M. Zhong, R. Wang, K. Kawamoto, B.D. Olsen, J.A. Johnson, Quantifying the impact of molecular defects on polymer network elasticity, Science 353 (2016) 1264.
[43] A. Koike, N. Nemoto, T. Inoue, K. Osaki, Dynamic light scattering and dynamic viscoelasticity of poly(vinyl alcohol) in aqueous borax solutions. 1. Concentration effect, Macromolecules 28 (1995) 2339–2344.
[44] N. Nemoto, A. Koike, K. Osaki, Dynamic light scattering and dynamic viscoelasticity of poly(vinyl alcohol) in aqueous borax solutions. 2. Polymer concentration and molecular weight effects, Macromolecules 29 (1996) 1445–1451.
[45] S. Biffi, R. Cerbino, F. Bomboi, E.M. Paraboschi, R. Asselta, F. Sciortino, T. Bellini, Phase behavior and critical activated dynamics of limited valence DNA nanostars, Proc. Natl. Acad. Sci. 110 (2013) 15633–15637.
[46] E. Bianchi, J. Largo, P. Tartaglia, E. Zaccarelli, F. Sciortino, Phase diagram of patchy colloids: towards empty liquids, Phys. Rev. Lett. 97 (2006) 1–4.